Korean J. Chem. Eng., **29**(3), 377-383 (2012)
DOI: 10.1007/s11814-011-0179-1

Photocatalytic degradation of benzene, toluene, ethylbenzene, and xylene (BTEX) using transition metal-doped titanium dioxide immobilized on fiberglass cloth

Laksana Laokiat*,, Pongtanawat Khemthong***, Nurak Grisdanurak****,†, Paiboon Sreearunothai*****, Wanwisa Pattanasiriwisawa******, and Wantana Klysubun******

*International Postgraduate Programs in Environmental Management, Graduate School, Chulalongkorn University, Bangkok 10330, Thailand
**NCE for Environmental and Hazardous Waste Management, Chulalongkorn University, Bangkok 10330, Thailand
***National Nanotechnology Center, National Science and Technology Development Agency, Pathumthani 12120, Thailand
****Department of Chemical Engineering, Faculty of Engineering, Thammasat University, Pathumthani 12121, Thailand
*****School of Bio-Chemical Engineering and Technology, Sirindhorn International Institute of Technology, Thammasat University, Pathumthani 12121, Thailand
******Synchrotron Light Research Institute, Nakhon Ratchasima 30000, Thailand
(*Received 31 March 2011 • accepted 13 July 2011*)

Abstract–Transition metal (Fe, V and W)-doped TiO_2 was synthesized via the solvothermal technique and immobilized onto fiberglass cloth (FGC) for uses in photocatalytic decomposition of gaseous volatile organic compounds--benzene, toluene, ethylbenzene and xylene (BTEX)--under visible light. Results were compared to that of the standard commercial pure TiO_2 (P25) coated FGC. All doped samples exhibit higher visible light catalytic activity than the pure TiO_2. The V-doped sample shows the highest photocatalytic activity followed by the W- and Fe-doped samples. The UV-Vis diffuse reflectance spectra reveal that the V-doped sample has the highest visible light absorption followed by the W- and Fe-doped samples. The X-ray diffraction (XRD) patterns indicate that all doped samples contain both anatase and rutile phases with the majority (>80%) being anatase. No new peaks associated with dopant oxides can be observed, suggesting that the transition metal (TM) dopants are well mixed into the TiO_2 lattice, or are below the detection limit of the XRD. The X-ray absorption near-edge structure spectra of the Ti K-edge transition indicate that most Ti ions are in a tetravalent state with octahedral coordination, but with increased lattice distortion from Fe- to V- and W-doped samples. Our results show that the TM-doped TiO_2 were successfully synthesized and immobilized onto flexible fiberglass cloth suitable for treatment of gaseous organic pollutants under visible light.

Key words: Photocatalytic Degradation, BTEX, Transition Metal-doped TiO_2

INTRODUCTION

Volatile aromatic compounds such as benzene, toluene, ethylbenzene, and xylene (BTEX) are well-known as major components of both indoor and outdoor air contaminants. Most aromatic hydrocarbons are potentially toxic, mutagenic or carcinogenic to humans [1]. This has stimulated interest worldwide to treat BTEX, especially at points of generation prior to its emission into the environment. Various methods have been investigated for controlling BTEX such as adsorption, condensation, thermal decomposition, catalytic incineration, biofiltration, and photocatalytic oxidation [2]. Among them, photocatalytic oxidation using TiO_2 seems to have the greatest potential, especially in the field of air treatment at low temperature. It is rapid, energy efficient, and effective for destruction of a wide range of organic air pollutants [3]. However, TiO_2 exhibits high catalytic activity only under UV light with energy larger than the TiO_2 band-gap energy (~3.0-3.2 eV), and is thus less useful for air treatment under natural ambient light [3].

To improve the photocatalytic activity and the response in the visible region, doping of TiO_2 with metals and non-metals was proposed [4,5]. Transition metals such as Cr, Mn, Fe, Co, Cu and Ni have been employed as dopants [6]. Among numerous transition metals, Fe, V, and W were chosen for this study because they have similar ionic radii to that of the Ti cation (Ti^{4+}=74.5 pm, Fe^{3+}=78.5 pm, W^{6+}=74 pm, and V^{5+}=68 pm), and are thus likely to be well dispersed into a TiO_2 matrix without phase segregation [7]. This can result in more effective enhancement of visible light absorption and photocatalytic activity than when metal dopant oxides are phase separated from the TiO_2 [8]. However, the activity depends on several factors such as dopant concentration, location, and distribution of dopants and their electronic configuration [8].

Powdered TiO_2 is perhaps the most common form of TiO_2 catalysts. However, its utilization can be quite cumbersome, unless the catalysts are immobilized onto suitable substrates such that they can be easily handled and recovered after pollutant treatment. Various types of materials including activated carbon filters [9], nonwoven textiles [10] as well as cotton fabrics [11] have been developed for the immobilization of TiO_2 photocatalysts, since substrate materials have been shown to influence activity of catalysts. Fiberglass cloth (FGC) is a promising material for use as a support of catalysts, especially for treatment of gaseous pollutants by TiO_2 because of its

†To whom correspondence should be addressed.
E-mail: gnurak@engr.tu.ac.th

resistance to photocatalytic decomposition, high mechanical strength, good flexibility, environmentally friendly, high temperature and fire resistance, which are suitable for industrial processes. Currently, few papers have reported the use of flexible, fire-resistance FGC as substrate material for TiO_2 [12] especially for photocatalytic treatment of air pollutants under visible light.

The present study aims to investigate the feasibility of applying Fe, V, and W-doped TiO_2 to treat gaseous BTEX under visible light. The Fe, V, and W were introduced into TiO_2 using sol-gel synthesis followed by solvothermal treatment. The resulting powders were then immobilized onto FGC. Samples were characterized using X-ray diffraction spectrometer (XRD), transmission electron microscopes (TEM), UV-Vis diffuse reflectance spectroscopy (UV-DRS), and X-ray absorption near-edge structure (XANES) to obtain information on phase components, particle and crystallite sizes, optical absorption, and oxidation state, and local geometry of the Ti atoms. Our tests on the prepared catalyst-coated FGC, using a home-made reactor equipped with a daylight fluorescent bulb show successfully a high removal efficiency of gaseous BTEX, results of which will be discussed.

EXPERIMENTAL SECTION

1. Preparation of Fe-, V-, and W-doped TiO_2

Transition metals (Fe, V, and W)-doped TiO_2 catalysts were prepared by the solvothermal method using $Fe(NO_3)_3 \cdot 9H_2O$, NH_4VO_3, and $Na_2WO_4 \cdot 2H_2O$ as metal sources at a concentration of 0.1% molar ratio to titanium tetraisopropoxide (TTIP). The synthesis was started by solvolysis of the TTIP and metal ions with isopropyl alcohol (IPA) in the presence of polyethylene glycol (PEG). This method was modified from a previous work described in the literature [13]. Pristine fiberglass cloth was heat-treated in an electric furnace at 500 °C (5 °C/min.) for 2 hours before immobilization of the catalysts to ensure complete removal of any organic residuals, and then cut into pieces of equal size. The immobilization was done by dispersing 1 g of the prepared catalysts in acetone followed by addition of an equal amount of epoxy resin under constant agitation until uniformly mixed and then coated onto the FGC by spray coating. The coated FGC was then calcined at 450 °C for 1 hour at a heating rate of 2 °C/min. The amount of coated catalysts on FGC was controlled to be the same at around 0.3 mg/cm^2 for all prepared samples.

2. Characterization of Catalysts

The V, Fe and W contents of the sample (shown in Table 1) were determined using atomic absorption spectroscopy (AAS). X-ray diffraction (XRD) patterns of the catalyst-coated FGC samples were obtained with an X-ray diffractometer (Bruker D8, angular resolution<0.005°, reproducibility<0.001°) equipped with a Cu-K_α radiation source (wavelength 1.5406 Å). The percentage of anatase and rutile in the sample was estimated from the areas covered by the dominant rutile [110] peak and the anatase [101] peak. The crystallite size of each phase was determined from broadening of the respective X-ray spectral peaks by the Scherrer formula. The XRD patterns were repeated three times in order to confirm slight shifts discussed in the results section. UV-Vis diffuse reflectance spectra (UV-DRS) were measured by UV-Vis diffuse reflectance spectrophotometer (Hitachi U-3010). The range of wavelengths measured was from 200 to 800 nm employing the pure powder of $BaSO_4$ as a reference. The local geometry of Ti in V, Fe and W-doped TiO_2 was studied by XANES at beamline 8 of the Synchrotron Light Research Institute (Public Organization), Thailand. Details of the set-up are described elsewhere [14]. In brief, XANES spectra were taken at room temperature in fluorescent mode using a 13-element Ge detector with double Ge (220) crystal monochromators for selection of photon energy. Incident photon intensity was monitored by an ion chamber filled with argon gas. Titanium metallic foil was used for calibration of photon energy at its *K*-edge transition. The absorbances at the edge jump of all samples were in the range of 1-2 in order to ensure good signal-to-noise ratio. The obtained spectra were processed and corrected for background absorptions using the Athena program [15]. Spectra were normalized following the procedure of Farges et al. [16] by dividing the pre-edge intensity with the atomic absorption in the post-edge region in order to make a comparison between the Ti local coordination and geometry in our results to those extensively classified in their work.

3. Photocatalytic Testing

The photocatalytic oxidation of BTEX was carried out in a gas phase batch reactor as shown in Fig. 1. There are three main parts of the reactor: the BTEX saturators (A), the humidifier (B) and the catalytic reaction vessel. The reaction vessel contains three concentric cylinders made of borosilicate glass. Each layer is sealed from each other. The outermost layer is for temperature control by means of water circulation, or vacuum pumping. The innermost layer, or the central core, houses the light source (Toshiba, FL18W/T8/EX-D fluorescent daylight lamp, λ_{max}~425 nm). The middle layer is the section where gas flows and catalytic reactions take place. The flexible catalyst-coated FGC is inserted into this section by wrapping around the outside surface of the central core, and is thus in direct contact with the gas in the middle layer. The light intensity at the surface of the FGC was 58 W/m^2 as determined by a power meter

Table 1. Characteristic properties of the prepared catalysts

Catalysts	Anatase : Rutile	Metal content[a]	Crystallite size (nm)[b]	Average particle size (nm)[c]	Band-gap energy (eV)	Toluene removal efficiency
TiO_2 (P25)	83 : 17		5	26	3.28	21%
Fe-TiO_2	81 : 19	0.87	5	72	3.14	48%
W-TiO_2	87 : 13	0.93	7	52	2.90	54%
V-TiO_2	90 : 10	0.85	6	46	2.90	69%

[a]Determined by AAS

[b]Determined from broadening of XRD peaks using Scherrer equation

[c]Determined from TEM images

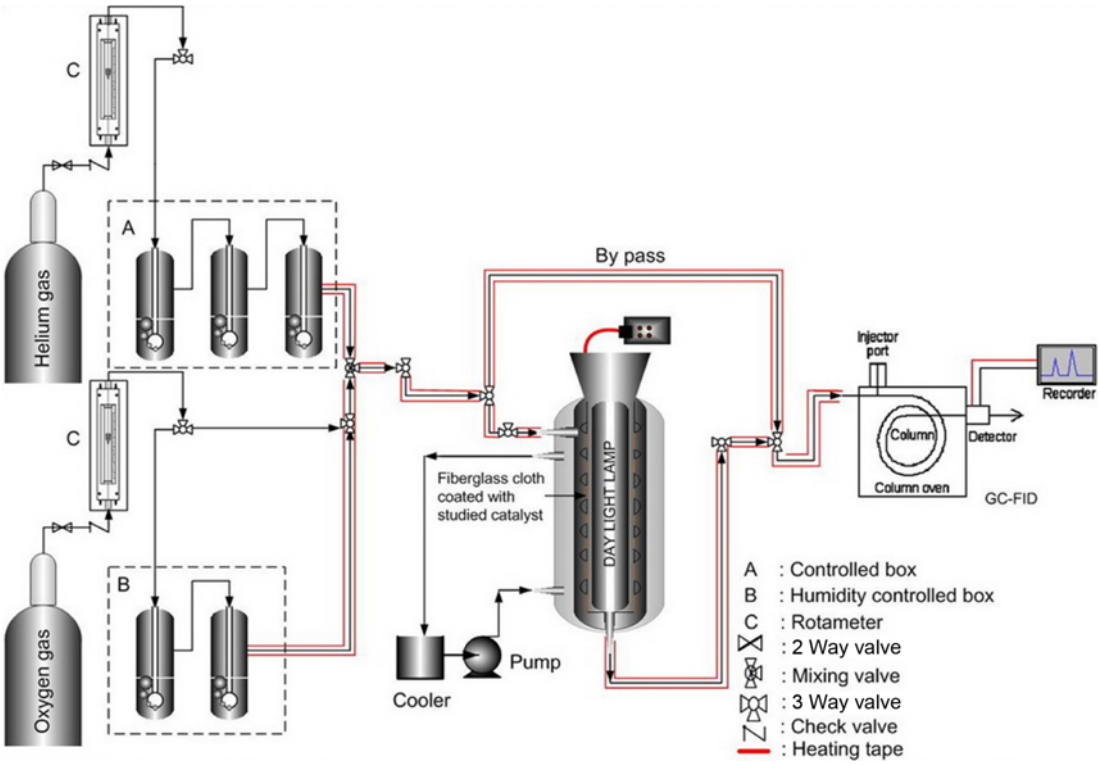

Fig. 1. Schematic diagram of the set up used for photocatalytic degradation test of the BTEX gases by the prepared catalyst-coated FGC.

(Kimo Solarimeter SL100). The BTEX vapors are generated from the saturators by bubbling helium gas through a series of three glass saturators containing BTEX liquid. Its concentration can be controlled by adjusting the temperature of the saturators and the flow rate of dilution gas (pure oxygen). Oxygen gas was used as an electron acceptor forming hydroxyl radicals. The oxygen gas molar concentration was controlled by dilution with helium gas to be around 21% in order to simulate a similar amount of oxygen as that found in normal atmospheric air. The batch reactor was flushed and filled with pure oxygen prior to introduction of BTEX vapour. The controlled amount of BTEX vapour was allowed to mix with the oxygen gas that had 30% relative humidity, and the mixture flowed through the reactor for 2 hours in the dark to attain equilibrium adsorption. Once the polluted air concentration stabilized, the inlet valve to the vessel was closed and the lamp was turned on. The BTEX concentrations were recorded against the illumination time throughout the test. All BTEX concentrations at the sampling points were monitored by a gas chromatograph (GC 14A, Shimadzu) equipped with a flame ionization detector (FID) with a DB1 capillary column. The GC uses helium as a carrier gas with a column temperature of 50 °C, an oven temperature of 200 °C, and a detector temperature of 200 °C. The reference blank tests were carried out in two conditions at room temperature under atmospheric pressure using toluene to represent BTEX gas: one illuminated without catalyst and the other with P25-coated FGC catalyst but without irradiation. In all experiments, the BTEX concentration was controlled in the range of 1,000-1,200 ppm with catalysts loaded on FGC at 0.30 mg/cm^2. Samples were collected at time intervals of 0, 30, 60, 90 and 120 minutes. The blank-test results showed that the toluene concentration after 120 minutes was similar to the initial toluene concentration, indicating

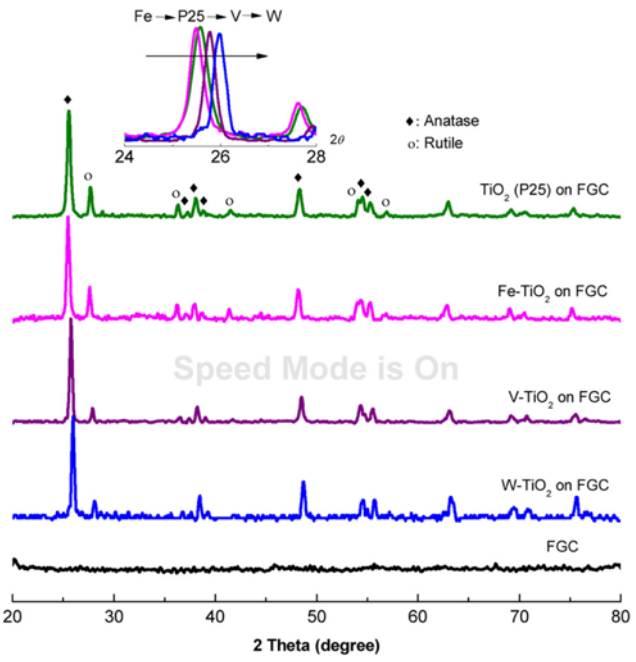

Fig. 2. XRD patterns (from bottom to top) of the FGC substrate, W-doped, V-doped, Fe-doped and pure TiO_2 (P25) immobilized on FGC. Peaks corresponding to the anatase and rutile phases of TiO_2 are marked by the solid diamond and open circle, respectively. The top insert plots the dominant anatase and rutile peaks from all samples on the same axis, showing the peaks of the V- and W-doped samples to shift slightly to higher angles, while the peaks of the Fe-doped sample to shift slightly to lower angles with respect to their corresponding peak positions of the pure TiO_2 (P25) sample.

that the toluene was not lost due to reactor leakage or adsorption.

RESULTS AND DISCUSSION

1. Characterization of Catalysts

Fig. 2 shows the XRD patterns of all metal-doped TiO_2 samples and P25 coated onto FGC. The spectra reveal that both anatase and rutile phases exist in all samples from their dominant peaks at around 25.6° (anatase [101] plane) and 27.7° (rutile [110] plane). No new peaks associated with crystalline phases of the dopant oxides were detected. This could be due to the fact that formation of dopant oxides is below the XRD detection limit or that the metal dopant ions are well substituted into the Ti ions due to their similar ionic radii [7]. A slight positive shift to higher angle was observed for the V- and W-doped samples, which may indicate slight lattice shrinkage of some of the TiO_2 lattices caused by substitution of the dopants. A smaller negative shift to a lower angle was also observed for the Fe-doped sample. This was possibly due to the slightly larger ionic radii and the lower charges of the Fe^{3+} compared to the Ti^{4+}. The lattice deformation for the V- and W-doped samples is also in agreement with results from XANES measurements, which is to be discussed later.

Utilizing the Scherrer equation [13], the average crystallite size of the two phases can be determined from broadening of the anatase and rutile peaks. The crystallite sizes as well as the anatase and rutile percentage are listed in Table 1. Our result shows that P25 contains approximately 4 : 1 anatase to rutile ratio, in agreement with usual values cited in the literature [17]. The TM-doped TiO_2 samples were observed to have quite small crystallite sizes, suggesting that the transition metal dopants may retard the growth of the TiO_2 crystalline phase and the transformation of anatase to rutile in accordance with several observations by others [18,19]. The large fraction of anatase to rutile can be beneficial for photocatalytic activity since the anatase phase has generally been shown to have higher photocatalytic activity than the rutile phase [20].

Information about local coordination and transition states of atoms in the samples can be further gained from the X-ray absorption near-edge structure (XANES) spectra of the samples. Fig. 3 shows the XANES spectra taken at the *K*-edge (s→p transition) of Ti atoms. The *K*-edge transition energies of all samples are at similar positions to that of the crystalline rutile and anatase TiO_2, indicating that most Ti ions in these samples are in the same tetravalent Ti^{4+} state as that in the pure TiO_2. The pre-edge structures of the anatase and rutile phases have been attributed to the weak dipole-allowed transition of the core electrons (1s) to the hybridized 3d-4p orbital states (labelled as A_2 and A_3) or to the hybridized 4p-4s states (B), and the quadrupolar transition of 1s to 3d orbitals (A_1) [16,21]. Usually, the degree of hybridization increases as the lattice loses its center of symmetry or is distorted, e.g., in going from octahedral to square pyramidal and tetrahedral lattices, resulting in higher intensity of the pre-edge structures. Previously, Farges et al. extensively categorized a range of Ti compounds for which Ti existed in various coordination states and showed that for Ti^{4+} in tetrahedral coordination (TiO_4), the normalized intensity of the pre-edge structures was usually in the range of 0.7-1.0, while for those in the square pyramidal (TiO_5) and octahedral (TiO_6) coordination, the pre-edge intensities were in the range of 0.4-0.7 and 0.05-0.4, respectively [16]. The normalized pre-edge intensity of all samples is in the range of 0.1 to 0.4, signifying that the majority of Ti ions in these samples are in the TiO_6 octahedral coordination.

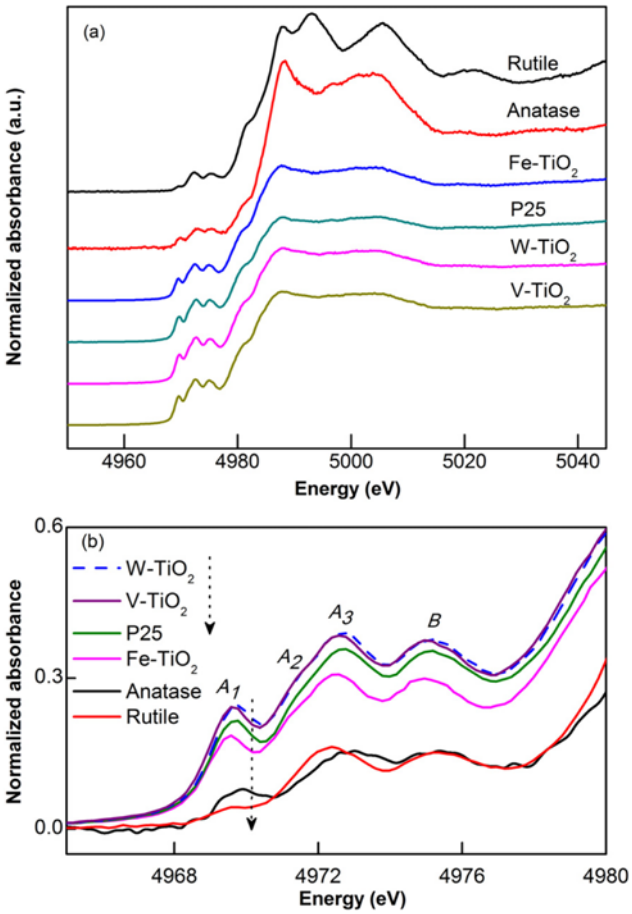

Fig. 3. (a) XANES spectra of the Ti *K*-edge in the prepared catalysts compared to those of the reference rutile and anatase TiO_2, (b) Close-up of the pre-edge region in (a) overlaid on the same scale to depict changes in the pre-edge intensity. From top to bottom (indicated also by a guiding arrow): W-doped, V-doped, P25, Fe-doped, anatase and rutile TiO_2.

A closer examination of the pre-edge intensities reveals that both the P25 and all TM-doped samples have higher pre-edge intensities than those of the pure anatase or rutile TiO_2. This indicates that Ti ions in the P25 and in the TM-doped samples are in the more distorted octahedral or less symmetrical environment than those in the pure crystalline rutile and anatase phases. There may be two reasons contributing to this. First, in the case of TM-doped samples, this is not surprising given that the TM dopants should cause some disorders in the TiO_2 matrix especially if they are well dispersed into the TiO_2 lattices and not segregated out as separate oxides. The V- and W-doped samples seem to show the highest increase in distortion, in agreement with the XRD results that the two dopants caused the largest shift in the XRD peaks. The second factor is possibly due to the coexistence of both rutile and anatase phases in these samples, as compared to single rutile or anatase phase samples. It is well known that insufficient thermal treatment partially transforms the anatase into the rutile phase, leading to coexistence of both anatase and rutile phases in the same particle. This has been shown by several

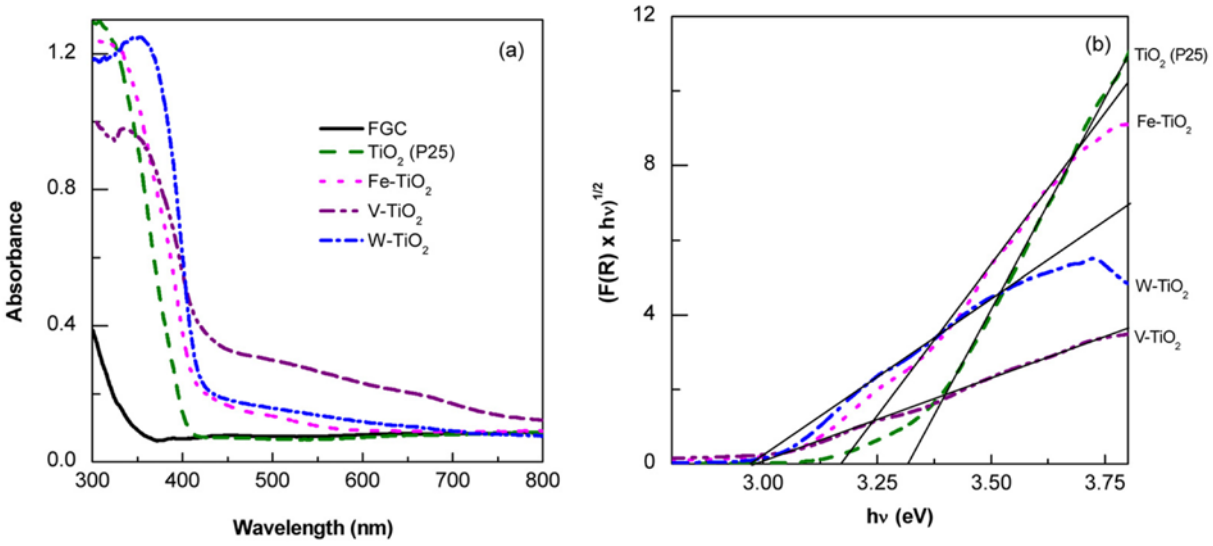

Fig. 4. (a) UV-Vis DRS spectra of the prepared catalyst-coated FGC samples and (b) the Kubelka-Munk transformation of (a) in order to obtain band-gap energies of the prepared catalysts.

works on both P25 [22], or other TM-doped TiO_2 [23,24] particles utilizing high-resolution TEM. The increased lattice disorder created at the boundary regions between the two phases can also contribute to the increase in the pre-edge intensity observed here.

Fig. 4 shows the UV-DRS measurements of all the TM-doped samples as well as the P25 coated onto FGC support. The absorption edges of all the doped samples are clearly shifted to the red compared to that of the pure TiO_2 (P25). The absorptions in the visible region (λ>400 nm) of all the doped samples are also higher than that of the pure TiO_2. The V-doped sample shows the highest absorbance in the visible region followed by the W-doped and Fe-doped TiO_2. This trend correlates also with the visible-light photocatalytic performance of each catalyst discussed in the next section.

To determine the band-gap energy more accurately than that inferred from an absorption edge, the UV-DRS spectra were transformed using the Kubelka-Munk method [25]. The resulting transforms are shown in Fig. 4(b). The intersection between the linear fit to the transformed curves and the energy axis yields the band-gap energies, which correspond to 3.28, 3.14, 2.90, and 2.90 eV for the P25, Fe-, W-, and V-doped TiO_2 samples, respectively. The absorption edge redshift as well as the increase in the visible region absorption of TiO_2 doped with transition metals is usually explained by the difference in energy levels between the dopants and the TiO_2 valence and conduction bands, resulting in reduced photoexcitation energy and thus band-gap energy [8].

2. Photocatalytic Testing

The photocatalytic activity was evaluated analyzing the percentage removal of BTEX under visible light at room temperature (25-

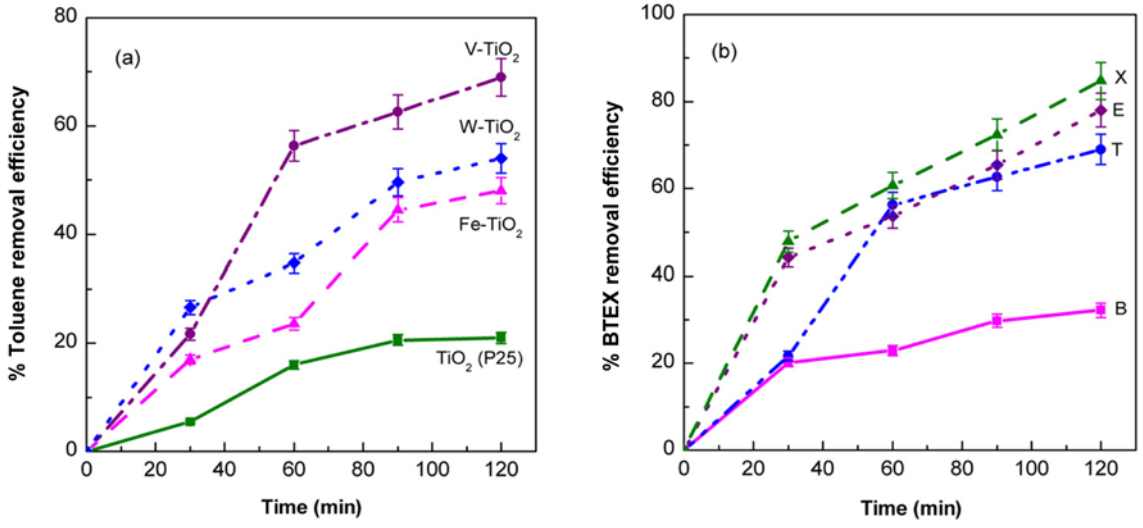

Fig. 5. (a) Percent removal efficiency of gaseous toluene as a function of time for each catalyst-coated FGC. After 120 minutes of visible light irradiation, the V-doped TiO_2 displayed the highest removal efficiency followed by the W-, Fe- and pure TiO_2. (b) Percent removal efficiency of each BTEX gas by the V-doped TiO_2. From the lowest removal efficiency to the highest: benzene (B), toluene (T), ethylbenzene (E), and o-xylene (X).

27 °C). The removal efficiency of BTEX was calculated using the equation,

$$\%\text{Removal} = \frac{[C]_{initial} - [C]_{final}}{[C]_{initial}} \times 100$$

where $[C]_{initial}$ is the initial BTEX concentration inside the reactor vessel and $[C]_{final}$ is the final BTEX concentration after 120 minutes of irradiation time. Toluene was first used as a representative gas to test for the catalytic activity across all the catalyst-coated FGC samples. The conversion of 21% was reached with the pure TiO_2 (P25), while the TM-doped catalysts exhibited much higher performance. The conversion of 48%, 54% and 69% was reached with Fe-, W- and V-doped TiO_2, respectively. The results are shown in Fig. 5(a). The increased catalytic activities seemed to correlate well with the order of increased visible light absorption of these catalysts (Fig. 4), following the same order of P25<Fe-doped<W-doped<V-doped TiO_2. These TM dopants appear to increase the absorption in the visible region of TiO_2 and can thus better utilize photons in the visible range for photocatalytic reactions. The surface area is also an important factor in determining activity. The average particle sizes obtained from TEM are shown in Table 1. We note that the P25, which has the smallest average particle size and thus is likely to have the largest surface area for reactions, actually showed minimal activity. This is most likely because of its inability to absorb and to utilize photon energy in the visible range. We note that other factors such as the recombination rates [26] could also be considered for deciding which dopant yields optimum performance. However, this process is beyond our current investigation.

Since the V-doped TiO_2 showed the highest performance in decomposing gaseous toluene, it was selected for degradation tests across other BTEX gases under similar conditions. The removal efficiency tests of each BTEX gas by the V-doped TiO_2 were performed with the initial concentrations of 862, 1,163, 785, and 965 ppm for the benzene, toluene, ethylbenzene, and o-xylene gases, respectively. The results depicted in Fig. 5(b) reveal that the o-xylene gas was removed most efficiently followed by the ethylbenzene, the toluene, and the benzene gases. This trend seems to correlate well with the gas-phase ionization potential (IP) of each BTEX gas, which increases from o-xylene (8.56 eV), to ethylbenzene (8.77 eV), to toluene (8.83 eV), and benzene (9.24 eV). Benzene has the highest IP and thus is the most difficult species to be oxidized [27]. This is probably due to the fact that benzene structure is chemically more stable than the other BTEX gases.

CONCLUSIONS

Transition metal (Fe, W, V)-doped TiO_2 catalysts were successfully synthesized using solvothermal method and immobilized onto flexible fiberglass cloth for treatment of BTEX gases. The obtained catalysts exhibited mixed rutile-anatase phases. All dopants appeared to be well dispersed in the TiO_2 matrix, and no new peaks associated with dopant oxides could be detected in the XRD spectra. The V and W dopants caused the XRD peaks of TiO_2 to shift slightly to higher angles, while the Fe dopant caused a small negative shift, indicating that a certain fraction of TiO_2 lattices were deformed by introduction of the dopant atoms. This is in good agreement with the results from XANES measurements, showing that the TM dopants caused the increase in pre-edge intensity, suggesting for a less symmetrical octahedral environment around the Ti atoms. All TM-doped samples exhibit increased visible absorption compared to that of the pure TiO_2, with the V-doped TiO_2 showing the highest increase, followed by the W- and Fe-doped TiO_2. For photocatalytic degradation of gaseous toluene, V-doped TiO_2 showed the highest efficiency followed by W- , Fe- and the un-doped TiO_2 (69%, 54%, 48%, and 21%, respectively). This is probably due to the effect of the highest increase in the visible light absorption and also the smallest particle size among the doped samples of the V-doped TiO_2. Among BTEX gases, o-xylene displays the highest removal efficiency followed by ethylbenzene, toluene, and benzene correlating with the trend in their ionization potentials (increasing from o-xylene to benzene). Our results show that TM-doped TiO_2 immobilized on flexible fiberglass cloth is suitable for applications in photocatalytic treatment of gaseous BTEX under visible light.

ACKNOWLEDGEMENTS

The authors acknowledge Office of the Higher Education Commission, Thailand, for the financial support.

REFERENCES

1. S. Wang, H. M. Ang and M. O. Tade, *Environ. Int.*, **33**, 694 (2007).
2. C. Collins, F. Laturnus and A. Nepovim, *Environ. Sci. Pollut. Res. Int.*, **9**, 86 (2002).
3. R. Thiruvenkatachari, S. Vigneswaran and I. S. Moon, *Korean J. Chem. Eng.*, **25**, 64 (2008).
4. B.-Y. Lee, S.-H. Park, S.-C. Lee, M. Kang, C.-H. Park and S.-J. Choung, *Korean J. Chem. Eng.*, **20**, 812 (2003).
5. T. Ohno, M. Akiyoshi, T. Umebayashi, K. Asai, T. Mitsui and M. Matsumura, *Appl. Catal. A: Gen.*, **265**, 115 (2004).
6. O. Carp, C. L. Huisman and A. Reller, *Prog. Solid State Chem.*, **32**, 33 (2004).
7. R. D. Shannon, *Acta Crystallogr. A.*, **32**, 751 (1976).
8. M. Anpo, S. Dohshi, M. Kitano, Y. Hu, M. Takeuchi and M. Matsuoke, *Annu. Rev. Mater. Res.*, **35**, 1 (2005).
9. C. H. Ao and S. C. Lee, *Appl. Catal. B: Environ.*, **44**, 191 (2003).
10. Y. Ku, C. Ma and Y. Shen, *Appl. Catal. B: Environ.*, **34**, 181 (2001).
11. Y. Dong, Z. Bai, R. Liu, X. Wang, H. Yan and T. Zhu, *Environ. Technol.*, **27**, 705 (2006).
12. Y. S. You, K.-H. Chung, J.-H. Kim and G. Seo, *Korean J. Chem. Eng.*, **18**, 924 (2001).
13. K. Wantala, L. Laokiat, P. Khemthong, N. Grisdanurak and K. Fukaya, *J. Taiwan Inst. Chem. Eng.*, **41**, 612 (2010).
14. P. Khemthong, W. Klysubun, S. Prayoonpokarach and J. Wittayakun, *Mater. Chem. Phys.*, **121**, 131 (2010).
15. B. Ravel and M. Newville, *J. Synchrotron Rad.*, **12**, 537 (2005).
16. F. Farges, Jr. G. E. Brown and J. J. Rehr, *Phys. Rev. B.*, **56**, 1809 (1997).
17. B. Ohtani, O. O. Prieto-Mahaney and D. L. R. Abe, *J. Photochem. Photobiol. A.*, **216**, 179 (2010).
18. C. Y. Wang, C. Bottcher, D. W. Bahnemann, J. K. Dohrmann, *J. Mater. Chem.*, **13**, 2322 (2003).
19. J. Choi, H. Park and M. R. Hoffmann, *J. Phys. Chem. C.*, **114**, 783 (2010).

20. A. Fujishima and X. Zhang, *C.R. Chimie*., **9**, 750 (2006).
21. Z. Y. Wu, G. Ouvrard, P. Gressier and C. R. Natoli, *Phys. Rev. B*., **55**, 10382 (1997).
22. J. Zhou, M. Takeuchi, A. K. Rayc, M. Anpo and X. S. Zhao, *J. Colloid Interface Sci*., **311**, 497 (2007).
23. B. I. Lee, S. Kaewgun, W. Kim, W. Choi, J. S. Lee and E. Kim, *J. Renewable Sustainable Energy*, **1**, 23101 (2009).
24. Y. Zhang, S. Wei, H. Zhang, S. Liu, F. Nawaz and F. S. Xiao, *J. Colloid Interface Sci*., **339**, 434 (2009).
25. E. Kanchanatip, N. Grisdanurak, R. Thongruang and A. Neramittagapong, *Reac. Kinet. Mech. Cat.*, **103**, 227 (2011).
26. A. D. Paola, S. Ikeda, G. Marci, B. Ohtani and L. Palmisano, *Int. J. Photoenergy*, **3**, 171 (2001).
27. National Institute of Standards and Technology Chemistry WebBook (2010). http://webbook.nist.gov/chemistry/. Accessed 12 January 2011.